Research Article

Ata El-Kareim Shoeib, Ahmed Noureldean Mohamed Arafa, Ramy Abd El-Hakeem Abd El Rady*, and Waleed Mohamed Fouad Tawhed

Experimental and analytical study on the behavior of hybrid GFRP/steel bars in reinforced concrete deep beams

https://doi.org/10.1515/cls-2022-0012
Received Nov 11, 2021; accepted Feb 03, 2022

Abstract: The deep beam is one of the essential members of high-rise buildings structures, so the deep beams are used as a transfer girder; in walls water structures, the deep beam behavior is different from the slender beam behavior; the deep beam plane section before does not remain plane after bending. In recent years, the use of FRP as a composite material in reinforced concrete structures has been growing up to cover problems by weight of structure buildings, corrosion, repairing, and construction cost. This paper presents an experimental, analytical study to assign the variation of mechanical properties of reinforced concrete deep beams using vertical and horizontal GFRP stirrups. This paper investigates the mechanical properties of test specimens for deep beams reinforced in shear with GFRP or steel bars as web reinforcement. The deep beams are reinforced with glass fiber reinforced polymer (GFRP) in various ratios as a web reinforcement configuration (0, 0.25%, and 0.40%) rather than traditional steel web reinforcement. All tested specimens have the same span to depth ratio of 0.40 (a/d); the primary and secondary reinforcement is steel bars. The web reinforcement ratio significantly affected deep beams' load capacity and mechanical behavior. The GFRP enhancement the mechanical behavior of the reinforced concrete deep. Increasing the GFRP web reinforcement ratio enhances the deep beam load capacity. The test results compared with the traditional ACI design method strut-tie model to demonstrate the effect of web reinforcement ratio on deep beam load capacity and strut width. The test results have been verified by ABAQUS 6.13.

Keywords: Hybrid reinforced concrete deep beams, deep beam, web reinforcement ratio of the deep beam, glass fiber reinforced polymer stirrups

1 Introduction

Reinforced concrete deep beams are used mainly for load transfer, such as transfer girders, bent caps, and pile caps. The reinforced concrete deep beams have an advantage over slender beams due to their resistance of a large magnitude of shearing force and normal stresses [1]. The slender beams and deep beams can transfer shear forces to supports through compressive stresses instead of the shear stresses. The diagonal cracks in the reinforced deep beams eliminate the inclined principal tensile stress required for beam action, and these diagonal cracks make a distribution of internal stress so, the deep beams act as tied arch [2]. These structural elements deteriorate due to freeze-thaw cycles and the corrosion of steel bars resulting from the large number of deicing salts used during the winter months in North America. Other circumstances, such as coastal weather, aggravate this phenomenon and exaggerate the hazard. Raw sewage is a source of causes corrosion of metallic components.

The advantages of FRP paved the way to use it in construction members such as columns, slabs, slender beams, and deep beams [3–5]. The over-hanging length beyond the support in the tested FRP-reinforced deep beams was relatively long to have a sufficient anchorage length for FRP longitudinal bars to prevent undesirable failure due to anchorage. However, the provided anchorage length used in the experimental studies is too long to be used in practice [1, 6, 7].

In the deep beams, the web reinforcement is significantly closer to the surface of the beam; then, the web reinforcement will be oversensitive to chemical exposure and an aggressive environment. The primary, secondary

***Corresponding Author: Ramy Abd El-Hakeem Abd El Rady:** Faculty of Engineering, Helwan University, Egypt; Email: rami.abdelhakeem@gmail.com

Ata El-Kareim Shoeib, Waleed Mohamed Fouad Tawhed: Civil Engineering Department, Helwan University, Egypt

Ahmed Noureldean Mohamed Arafa: Civil Engineering Department, Sohag University, Egypt

reinforcement is not hypersensitive as web reinforcement to chlorides and chemical exposure. In addition to that, the FRP can control crack width to avoid chloride migration to the inner reinforcement [8–10]. Thus, the present research proposal investigates incorporating FRP bars as web reinforcement mats in deep beams while maintaining the main reinforcement bars. This technique reduced maintenance costs because only the maintenance will be for primary reinforcement, facilitating repairing processes.

As previous research indicates, the steel web reinforcement in reinforced concrete deep is considered essential for crack control [11]. Nevertheless, there are odds between codes prevision and researchers about the effect of steel web reinforcement on the strength of reinforced concrete deep beams. For instance, other researchers reported that the steel web reinforcement improved the strength of the inclined strut and the shear strength of concrete deep beams [12]. Birrcher *et al.* 2013 [13] indicate that the strength of reinforced concrete deep beams is not affected by the web reinforcement. Moreover, providing the minimum steel web reinforcement in a reinforced concrete deep beam designed according to ACI 318 (2014) [14] would increase the capacity by 1.67 over the load capacity of a deep beam without steel web reinforcement.

2 Methodology

The methodology used in this study is experimental with theoretical validation. The experimental program used glass fiber reinforced polymer as web reinforcement rather than steel web reinforcement. Experiments were conducted on seven reinforced concrete beams to understand better the behavior of deep concrete beams reinforced with glass fiber reinforced polymer as web reinforcement and longitudinal steel bars. Finally, the verification of experimental results was varied using theoretical analyses based on ACI 318-19 [15], ACI 440.1R-03 [16], and ABAQUS.

3 Experimental program

3.1 Description of test specimens

Seven reinforced concrete beams were cast with rectangular cross-sections, sized 120 mm (width) × 800 mm (height) × 1170 mm length; Figure 1 shows the details of tested specimens. Figure 1 shows the reinforcement used in all specimens: two bars of 16 mm diameter, four bars of 12 mm

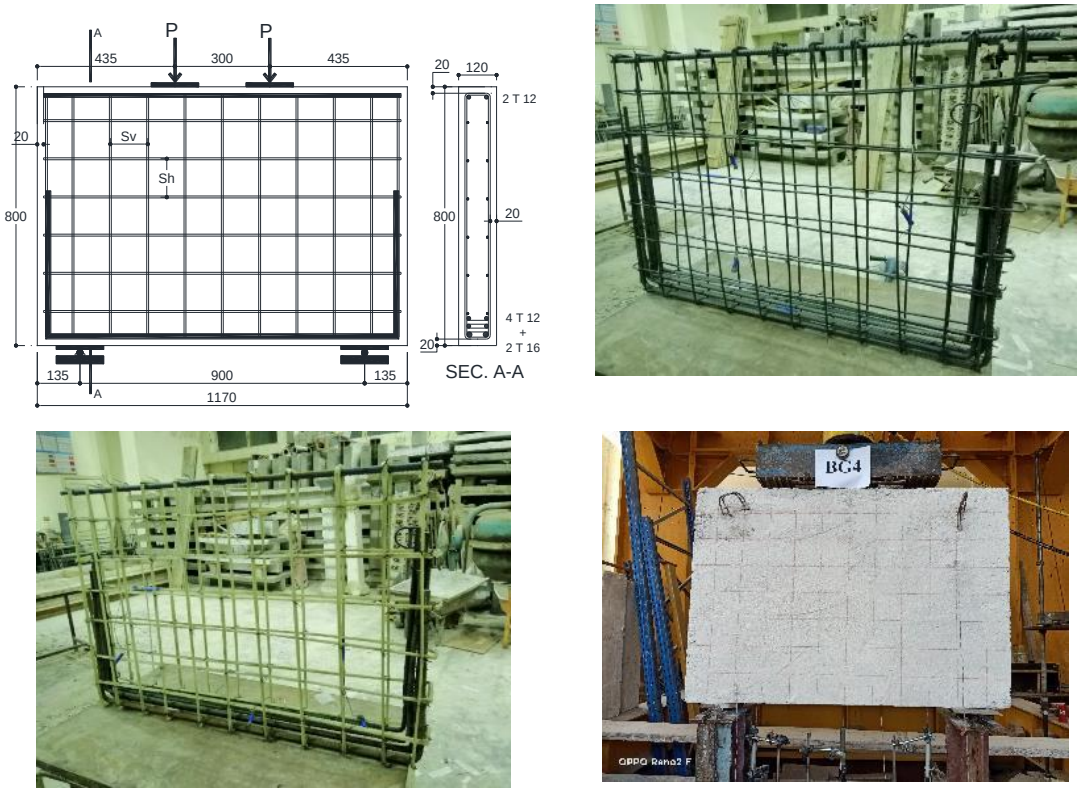

Figure 1: Details of a typical specimen

Table 1: Specimen's reinforcement details

Group	Specimen ID	Web reinforcement	S_h	S_v	ρ_h %	ρ_v %
A	BS1	Steel	0	0	0	0
	BS2		188	188	0.25	0.25
	BS3		118	118	0.40	0.40
B	BG1	GFRP	0	118	0.00	0.40
	BG2		118	0	0.40	0.00
	BG3		118	118	0.40	0.40
	BG4		188	188	0.25	0.25

diameter in the bottom reinforcement, and two bars of 12 mm diameter in the top reinforcement. The laboratory saw the casting of two groups of reinforced concrete deep beams. The exception is the control beam, which has no web reinforcement. The first group consists of three beams with varying steel web reinforcement ratios, except the control beam. Second, this group has four beams, each with a different glass fiber-reinforced polymer web reinforcement. Table 1 below contains information about the tested specimens (1).

3.2 Material properties and mix preparations

For all tested R.C beams, concrete compressive strength was equal to 25 Mpa consisting of Portland cement, equivalent to ASTM C150/C150M-15, natural aggregates, and natural water. The mixing of the concrete component, such as dolomite, sand, and cement, was performed using a drum mixer with a capacity of 0.125 m^3 in a dray mix; then, the water was added gradually to the mix; while mixing stayed with concrete became homogeneous. The cast of specimens were in slabs formworks. All specimens were cured for seven days and then removed from the formwork and stored until testing. For each mix, three cubes with dimensions 150×150×150 mm and three cylinders with 150×300 mm dimensions were taken during the cast of deep beams to specify the concrete strength. The cubes and cylinders were tested after 7 and 28 days to specify the concrete compressive strength. Table 2 illustrates the mixed proportions of the concrete. The yielding and ultimate stress for the steel was 360, 520 Mpa, respectively; Table 3 illustrates the properties of the GFRP.

Table 2: Concrete mix proportions (unit: kg/m^3)

Component	Concrete mix
Cement	350
Sand	630
Dolomite	1260
Water	175

Table 3: GFRP reinforcement bar properties

Bar diameter (mm)	Area (mm^2)	Tensile strength (Mpa)	Elastic modulus (GPa)
6	28.26	510	45

4 Instrumentation and testing procedure

4.1 Experimental setup and testing

The strain in the longitudinal reinforcing bar of 16 mm diameter was measurement by using electrical resistance strain gauge with a width of 5mm and length of 60mm. Two strain gauges were attached to each deep beam's longitudinal reinforcement bar and the web reinforcement. One strain gauge was attached to the length of the bar, and the other was attached to the web. The tested concrete deep beams were instrumented with linear variable differential transducers (LVDTs) to monitor deflection. The deflection of the deep beam during testing was measured using LVDTs, two of LVDTs located between the point of loading, support from left and right side of the deep beam, and one of LVDTs located at mid-span of the deep beam. All LVDTs were at the bottom of the reinforced concrete deep beam, as shown in Figure 3. The crack widths were measured manually with a 50×handheld microscope, and the crack formed between the load points and the supports identified these cracks.

Figure 2 depicts a typical test setup for tested specimens. The LVDT, load cell, and strain gauge readings are acquired automatically and displayed on a digital display unit. The crack formations were marked and recorded on the deep beam surface during the test until the failure. Mataria Faculty of Engineering, Helwan University, built a special 3D steel frame setup to test the beams. It consisted of I-beams connected with steel columns to support the beams during loading. There is a solid concrete floor beneath the steel columns. All tested specimens have the same dimension and spacing of 0.90 m between the supports center.

Figure 2: Test Setup

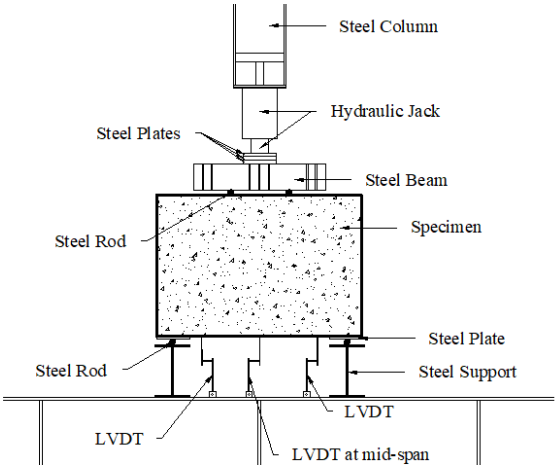

Figure 3: Details of the experimental setup

5 Test results and discussion

In this experimental and analytical study, all tested reinforced concrete deep beams have the same span to depth ratio of 0.40 (a/d). Analysis of all specimens presented using ABAQUS 6.13 and comparison with the experimental result

The structural analysis was applied using static analysis.

5.1 Crack pattern and mode of failure of tested specimens

Figure 4 depicts experimental specimens' crack patterns and failure modes after failure. The crack propagation for all experimental specimens is similar on the front and back sides of the concrete deep beam. The first crack for the concrete deep beams reinforced with steel web reinforcement was flexure, except BS2 was shear and flexural crack; the first crack appears within the range of 45-65% of the ultimate load. The first crack for the concrete deep beam with GFRP web reinforcement was flexural, except BG1 was a shear crack; the first crack appears within the range of 44-68% of the ultimate load. The flexural cracks formed between loading points are propagated vertically within an approximate range of 35-81% of the deep beam depth. Other flexural cracks propagated between the loading points as the load increased. The flexural crack width for the deep beam without web reinforcement is more comprehensive than web reinforcement. The first shear crack appeared for deep beam reinforcement with steel web reinforcement within 65-86% of ultimate load and within the range of 50-75% for deep beam reinforced GFRP as web reinforcement. The width and the number of shear cracks increased by load increasing. The main diagonal cracks through the expected diagonal strut at 95-100%, 87-100% of the ultimate load for groups A and B, respectively. The type of web reinforcement did not affect the number of bending cracks but affected shear cracks. The number of bending cracks for the deep beam with web reinforcement is less than that without web reinforcement. The ratio of web reinforcement did not affect the number of bending cracks.

The main diagonal shear crack extended with load increment toward the inner edge of the support plate and the outer edge of the loading point until specimens failed during the test. The other shear cracks stopped widening and propagating when the primary diagonal shear crack widened with the load increase. The specimens with steel web reinforcement had parallel cracks adjacent to the first

Figure 4: Crack development and mode of failure

main diagonal crack. Still, the concrete beam with a GFRP web reinforcement ratio of 0.40% only had parallel cracks adjacent to the first main diagonal crack. The main diagonal cracks and adjacent cracks are defined direction of the concrete diagonal strut, the concrete strut's width, and the concrete strut's shape. All experimental specimens were free of horizontal cracks. No premature failure occurred during the test. According to the results, crushing in the concrete diagonal strut was determined to be the failure mode of the experiment. The shape of the strut for the experimental specimens is prismatic shape except for BS2, BG3 is bottled shape.

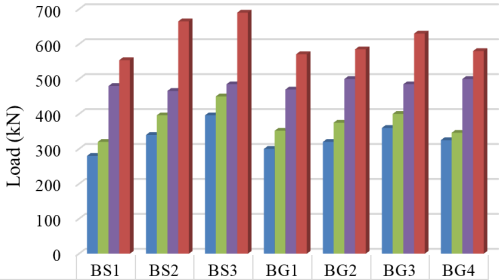

	BS1	BS2	BS3	BG1	BG2	BG3	BG4
First flexure crack load	280	340	396	300	320	360	325
First shear crack Load	320	396	450	352	375	400	346
Main diagonal crack load	480	466	485	470	500	485	500
Ultimate Load	554	665	690	571	585	630	580

Figure 5: Load for the experimental deep beam test result

5.2 Ultimate capacity

Figure 5 summarizes the test results obtained from testing specimens. It lists the load at ultimate, first flexure crack, first shear crack, main diagonal crack load for all specimens. The first flexure crack load is the first crack that occurred in the bending zone between loads; the main diagonal crack is the main shear crack formed and widened until the failure of the deep beam, the first shear crack load is the first shear crack occurred between loads and supports. The web reinforcement ratio does not affect the flexure crack loading during the test compared with the control deep beam without web reinforcement. Increasing the web reinforcement ratio in deep beams reinforced with steel web reinforcement increased the ultimate capacity of deep beams with steel web reinforcement, and for deep beam reinforced with GFRP as web reinforcement, a slightly enhancing in ultimate load was recorded, except for beam with web reinforcement ratio of 0.40%, comparing with control deep beam without web reinforcement. The first shear crack for a deep beam without web reinforcement was later than the first shear crack for other specimens. The deep beam with a web reinforcement ratio of 0.40% showed an enhancement in the shear crack load and main diagonal crack load than the other specimens. The steel web reinforcement increases the ultimate load within the range of 20-24.5% and 3-13.7% for the deep beam with GFRP web reinforcement, compared with the deep beam without web reinforcement.

5.3 Reinforced concrete deep beam load-deflection response

The deflection of the deep beam during testing was measured using three LVDTs, two of LVDTs located between the point of loading, support from the left and right side of the deep beam, and one of LVDTs located at the mid-span of the deep beam. All the LVDTs are at the bottom of the deep beam, and all specimens have the same deflection value at 20 kN. Mid-span deflection at maximum load of the reinforced concrete deep beam without web reinforce-

Table 4: Deflection of deep beams

Group	Specimen ID	ρ_h %	ρ_v %	$\Delta_{\text{at max.}}$	$\Delta_{\text{at failure}}$
A	BS1	0	0	3.609	7.640
	BS2	0.25	0.25	3.398	3.982
	BS3	0.40	0.40	2.284	3.027
B	BG1	0.00	0.40	2.826	7.707
	BG2	0.40	0.00	3.451	5.606
	BG3	0.40	0.40	3.000	3.339
	BG4	0.25	0.25	3.108	5.297

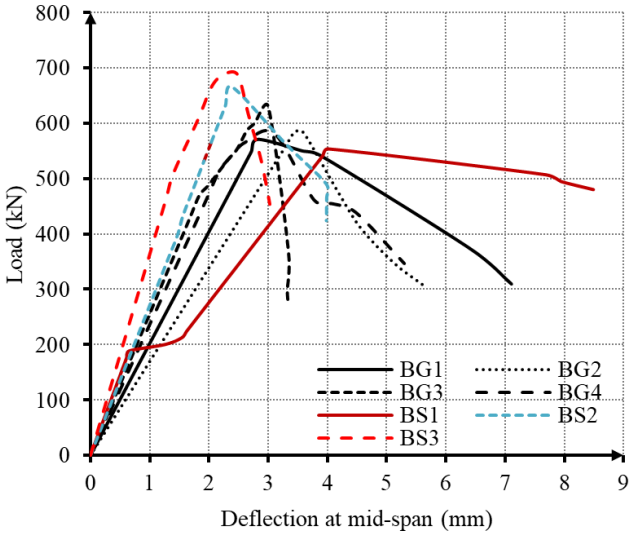

Figure 6: Load-deflection curve for deep beams

ment was 3.60 mm, while it was 2.39, 2.28 mm for the deep beam with steel web reinforcement ratio of 0.25, 0.40%; respectively, with the difference of 50% about the deflection for control deep beam without web reinforcement as shown in Figure 6. By increasing the steel web reinforcement ratio by 0.15%, the mid-span deflection was reduced by 17%. The deflection for deep beam reinforced with vertical, horizontal GFRP web reinforcement only decreased by 33, 10%; respectively, and 45, 50% for GFRP web reinforcement ratio 0.25, 0.40%; respectively, compared with control deep beam. With the increase of GFRP web reinforcement ratio of 0.15%, the total deflection at mid-span decreases by 21.5%, at maximum load. The increasing deflection for the deep beam with GFRP web reinforcement 0.25, 0.40% about 48, 58%; respectively, compared with the same deep beam reinforced with steel web reinforcement at the same ratio and load. All specimens exhibited a nearly bilinear up to failure.

5.4 Deformability factor and ductility energy index

Previous research mentioned many expressions to put a formula to measure the ductility from the energy absorption of the hybrid reinforced concrete deep beam. The area under the load-deflection curve is the energy absorption. The ductility energy ratio μ_E of hybrid GFRP reinforced concrete deep can be calculated from the following equation:

$$\mu_E = \frac{E_{\text{total}}}{E_{@0.75\text{p max}}} \tag{1}$$

Where μ_E, E_{total}, $E_{@0.75\text{p max}}$: are the ductility index, total energy absorption up to the failure load, and up to 75% of the maximum load, respectively. The displacement ratio from ultimate to maximum load defines the deformability factor (λ). In this paper, the ultimate load will equal 85% of the maximum load on the decreasing part of the load-deflection curve. The formula for the equation is as follows:

$$\lambda = \frac{\Delta_f}{\Delta_{max}} \tag{2}$$

In a concrete component, the transfer from mechanical energy to the inherent possible energy is referred to by the absorbed energy. The absorbed energy of concrete parts involves various composite processes, comprising plastic

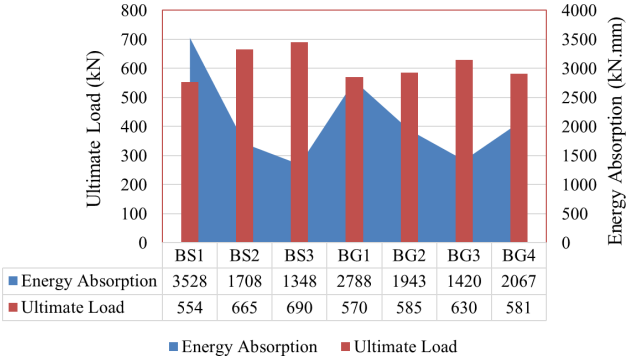

Figure 7: Energy absorption and ultimate load of tested specimens

Table 5: Ductility index and Deferability factor

Specimen ID	E_{total}	$E_{0.75p\,max}$	μ_E	Δ_f	Δ_{max}	λ
BS1	3528	255	13.85	8.490	4.011	2.12
BS2	1708	352.7	4.84	3.982	2.398	1.66
BS3	1348	359.9	3.75	3.028	2.284	1.33
BG1	2788	324.2	8.60	7.107	2.826	2.51
BG2	1943	354.8	5.48	5.606	3.452	1.62
BG3	1420	359.3	3.95	3.340	3.001	1.11
BG4	2067	294.9	7.01	5.298	3.109	1.70

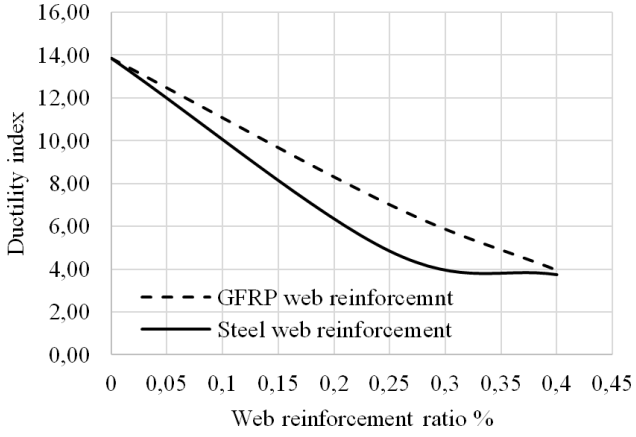

Figure 8: Relation between ductility index and web reinforcement ratio

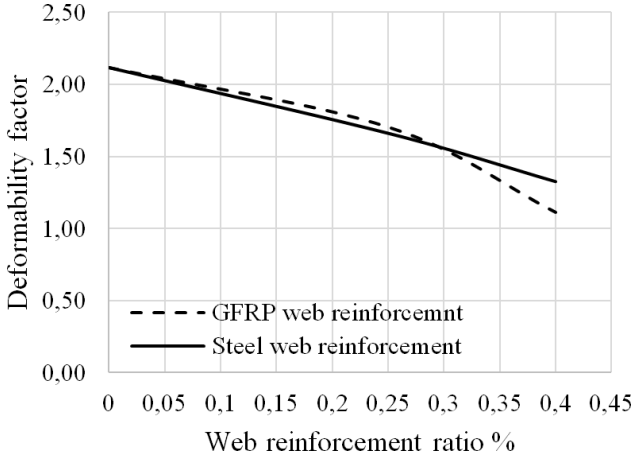

Figure 9: Relation between deformability factor and web reinforcement ratio

and elastic deformation and the rupture mechanics of crack propagation and initiation. The relation between web reinforcement ratio, deformability factor, and ductility index is illustrated in Figures 7-9 and Table 5.

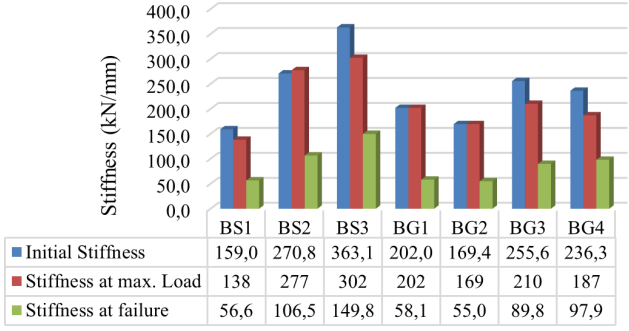

	BS1	BS2	BS3	BG1	BG2	BG3	BG4
Initial Stiffness	159,0	270,8	363,1	202,0	169,4	255,6	236,3
Stiffness at max. Load	138	277	302	202	169	210	187
Stiffness at failure	56,6	106,5	149,8	58,1	55,0	89,8	97,9

Figure 10: Stiffness of the deep beam specimens

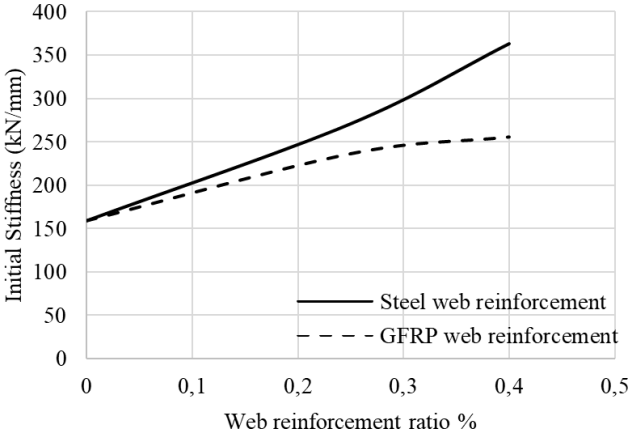

Figure 11: Relation between initial stiffness and web reinforcement ratio

5.5 Stiffness of the deep beam

The ability of a structural element to resist deformation or deflection as a result of an applied force is known as stiffness. Numerous parameters, including ductility, energy absorption, young modulus, and displacement, are influenced by stiffness. The increase of steel web reinforcement ratio had a significant effect on the stiffness of the deep beam. For a deep beam with steel web reinforcement, the initial stiffness and stiffness at the maximum load of deep beam increased by 70 to 128%, and for deep beam was re-

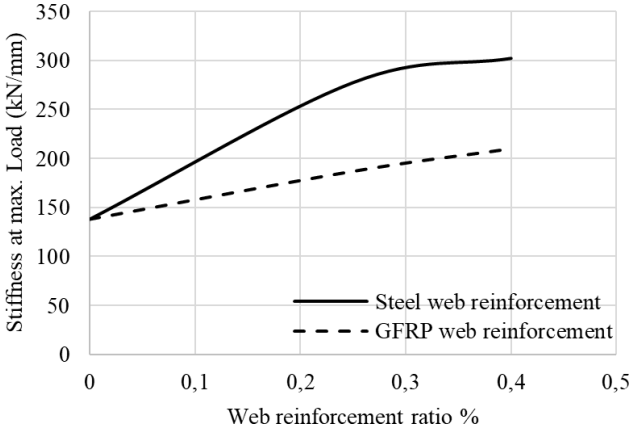

Figure 12: Relation between stiffness at max. Load and web reinforcement ratio

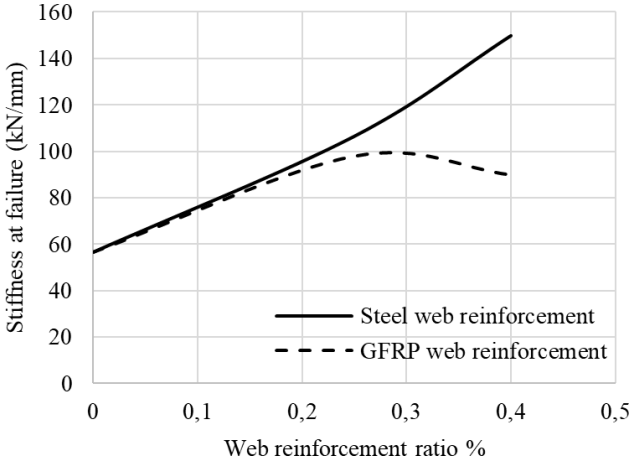

Figure 13: Relation between stiffness at failure and web reinforcement ratio

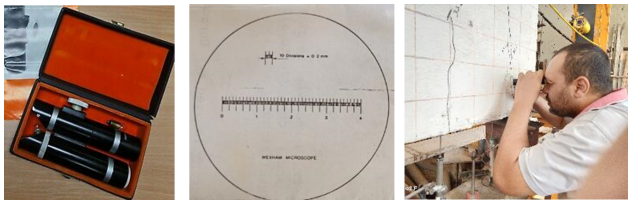

Figure 14: Wexham microscope and cracks width measurement

inforced by GFRP from 6 to 60% compared with a deep beam without web reinforcement. The stiffness at failure increased from 88 to 164% for the deep beam with steel web reinforcement and from 2.65 to 73% for deep beam reinforced with GFRP as web reinforcement, except BG2, no enhancement occurred in stiffness at failure, compared with deep beam without web reinforcement.

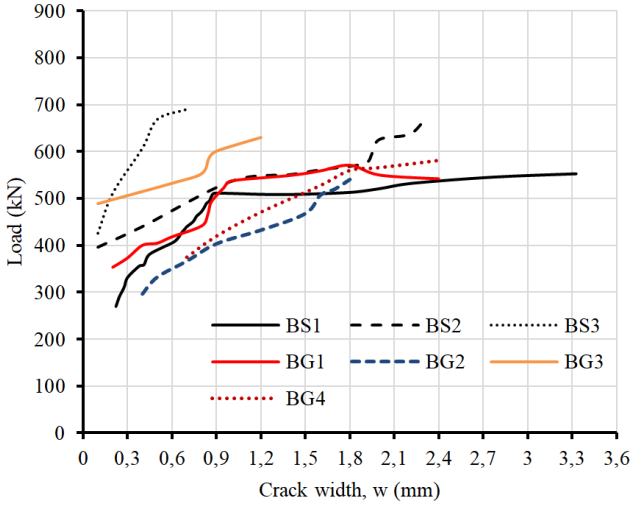

Figure 15: Crack width of tested specimens

5.6 Crack width

The crack width in the concrete deep beams was measured using the Wexham microscope; the microscope has a range of 4 mm measurement, divided into 0.2 mm divisions, subdivided into 0.02 mm divisions. The Wexham is a high-quality product designed to measure crack width in concrete; it consists of a high-definition microscope linked to an adjustable light source to provide a well-illuminated picture under good and bad working conditions, focusing the image is accomplished by turning the knurled knob on the microscope's side. The eyepiece graticule can be rotated through 3600 to align with the direction of the crack under examination.

The crack width was studied to explain the behavior of the concrete deep reinforced with hybrid GFRP/steel bars. The crack width was observed and recorded for main diagonal crack under load increasing for all tested specimens. In the numerical modeling, there was no record of crack width. The flexure cracks propagated at first and widened with a small range from 0.005 to 0.06 mm until the main diagonal crack formed, then the flexure cracks stopped widening, and the width of the main cracks increased with the load increasing until failure. The crack width for the beam with web reinforcement is less than wide from that without web reinforcement. At the same loading level, the concrete deep beam with a vertical reinforcement only gives less than the crack width of that reinforced with horizontal web reinforcement. The deep beam reinforced with GFRP as a vertical web reinforcement reduced the crack width by 27.8%, compared with the deep beam without web reinforcement, the deep beam reinforced with GFRP web reinforcement reduced the crack width by 45.8% from the total

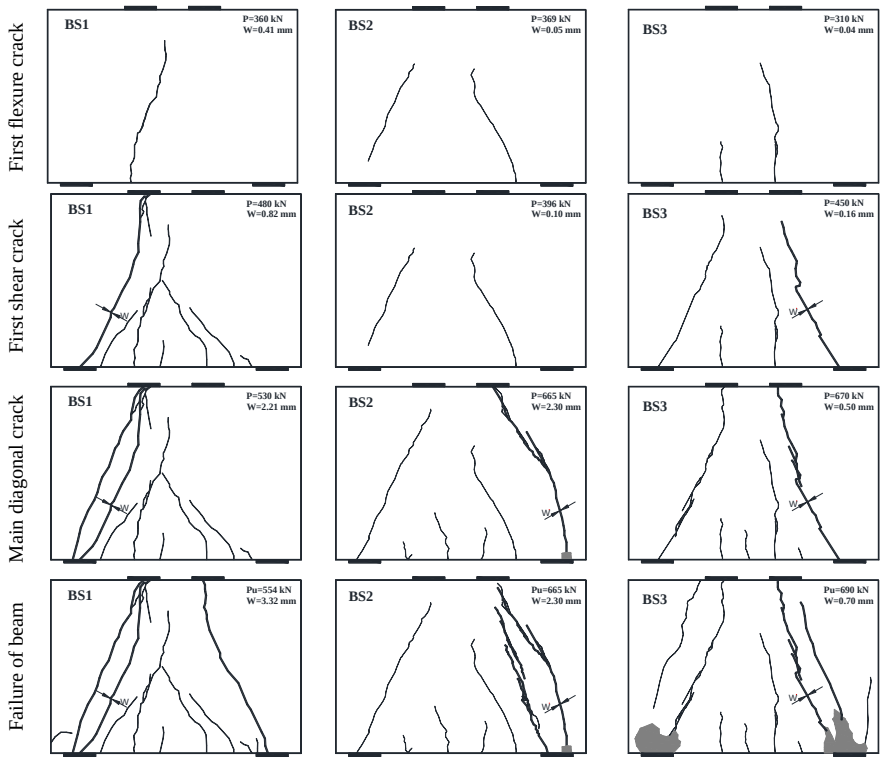

Figure 16: Crack development and mode of failure for the deep beam with steel web reinforcement

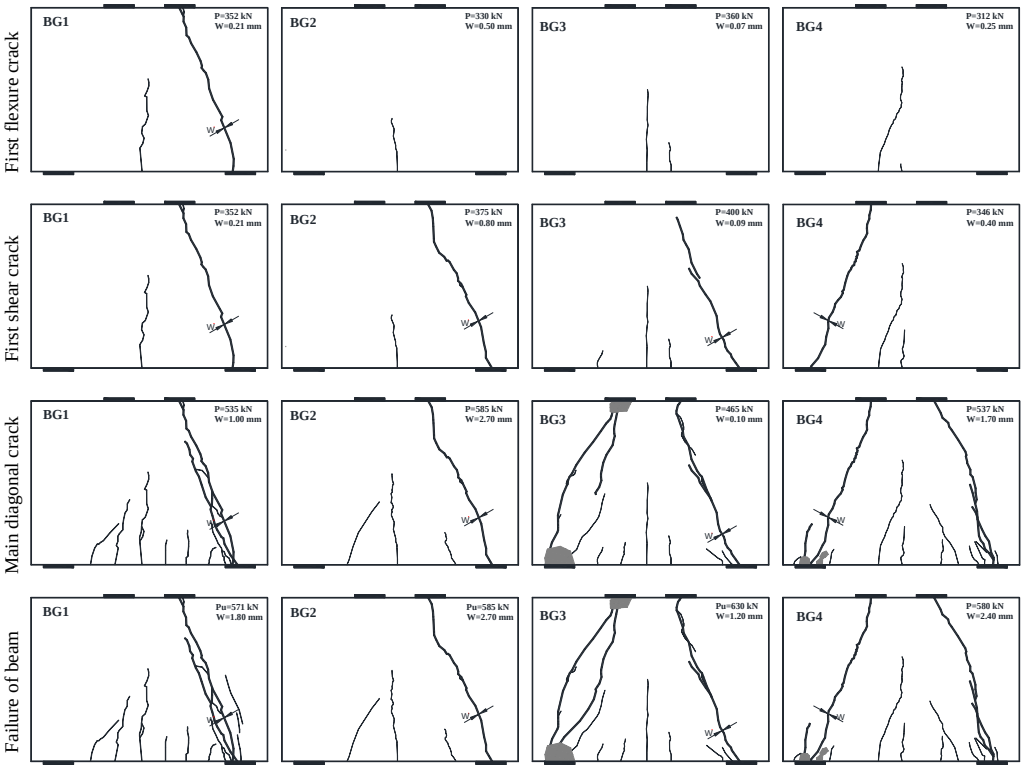

Figure 17: Crack development and mode of failure for the deep beam with GFRP web reinforcement

crack width of the deep beam without web reinforcement. The deep with horizontal and vertical steel web reinforcement, reduce the crack width within 30.7%, 78.9% for web reinforcement ratio 0.25%, 0.40%; respectively, reduction within 27.71%, 63.9% for deep beam reinforced with GFRP web reinforcement with ratio 0.25%, 0.40%; respectively. The GFRP web reinforcement plays a significant role in controlling the crack width, almost as steel web reinforcement is significant. Figures 16 and 17 illustrate the location of the measurement crack width.

5.7 Strains in longitudinal main reinforcement (tie)

Figure 18 shows the relation between strain and load in the main reinforcement bar with a diameter of 16 mm. The main bar has a strain gauge in the middle of it. For experimental deep beams, the relation was linear until the first flexure crack. The relation transformed to bilinear; no anchorage sign occurred during the specimens test. The specimens with GFRP web reinforcement take the same strain behavior for deep beams with steel web reinforcement until the maximum load point. The main reinforcement bars did not reach the point of yielding for all specimens. For a web reinforcement ratio of 0.40%, the main reinforcement bar has almost the same strain.

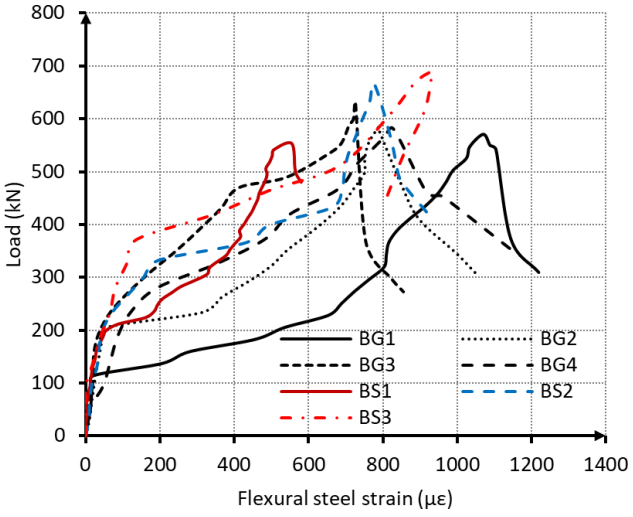

Figure 18: Strain curve for the main bar (Tie) of deep beams

5.8 Effect of hybrid bars on the strain of web reinforcement

Figure 19 illustrates the load-strain relationship for experimental deep beams. The deep beams with vertical web reinforcement only exhibited almost similar or slightly higher stiffness than the deep beam without web reinforcement; this is similar in stiffness, causing the experimental and numerical modeling to fail at nearly similar ultimate loads. In most cases, due to compression force in the concrete strut area, the stain in vertical web reinforcement exposed to be compression strain, and no degradation occurred in the concrete strut. In most cases, the higher strain in vertical web reinforcement was in the concrete diagonal. The vertical web reinforcement due to low strain compared with the deep beams that have horizontal web reinforcement

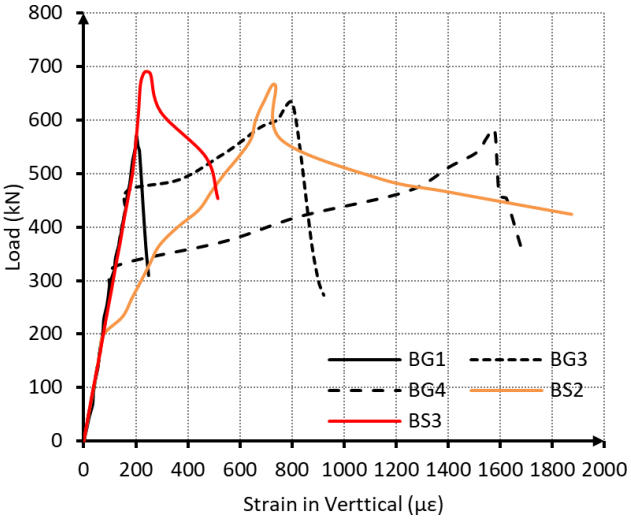

Figure 19: Strain curve of vertical web reinforcement for deep beams

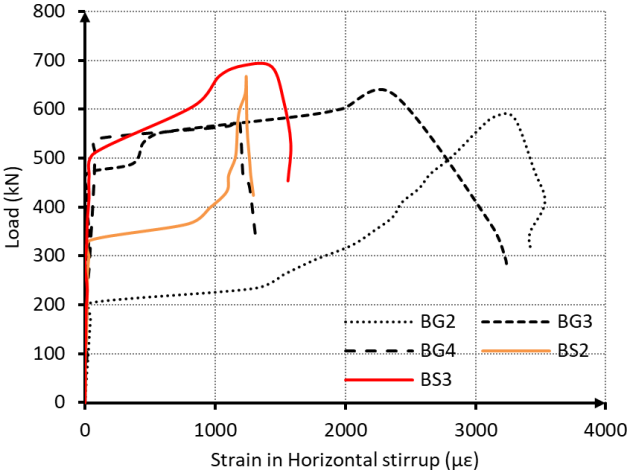

Figure 20: Strain curve of horizontal web reinforcement for deep beams

Table 6: Strain of deep beams

Specimen ID	Maximum strain in main steel at failure (με)	Maximum strain in main horizontal web reinforcement at failure (με)	Maximum strain in main vertical web reinforcement at failure (με)
BS1	580	—-	—-
BS2	917	1294	1874
BS3	811	1559	515
BG1	1219	—-	249
BG2	1049	3426	—-
BG3	855	3241	922
BG4	1156	1307	1689

only, the strength in the diagonal strut area did not increase, causing the same failure load of the concrete deep beam without web reinforcement. The increase of GFRP web reinforcement by 0.15% decreased the strain in deep beams reinforced with only vertical web reinforcement by 91%, by 45% for deep beam reinforced with vertical and horizontal web reinforcement, 72% for deep beams with deep beams steel web reinforcement. The vertical web reinforcement did not reach the point of yielding for all specimens.

Figure 20 shows the relation between load and strain for the experimental and numerical deep beam reinforced with horizontal web reinforcement to study the effect on concrete deep beam behavior. In tested specimens, the total strain in horizontal web reinforcement reaches twice the total strain in vertical web reinforcement. The increase of web reinforcement ratio by 0.15% decrease of strain within the range 23-34% for deep beams reinforced with GFRP web reinforcement, within the range 10-43% for deep beams reinforced with steel web reinforcement. The horizontal steel web reinforcement did not reach the point of yielding but occurred for GFRP web reinforcement, except BG4.

6 Prediction of the deep beam with various web reinforcement ratios based on equations

The capacity of the authors' predicted concrete deep beams was verified using available design equations, Kong *et al.*, strut-tie-model according to ACI 318-19 [15] (CAST Software), ACI traditional design method (ACI 318R-99) [17], and finite element method (ABAQUS 6.13). The authors summarized the equations used in each model in the following sections, followed by a comparison of experimental results and predicted ultimate shear capacity of tested specimens.

6.1 Kong *et al.* (1978)

Kong *et al.* [18] conduct an experimental study to predict the ultimate shear strength of a solid deep beam. The proposed equations to calculate the ultimate shear strength of a solid deep beam. This equation Eq. (3), calculates the web reinforcement ratio of solid beams with varying web reinforcement ratios.

$$V_n = Q_{ult} = C_1 \left[1 - 0.35\frac{x}{D}\right] f_t bD + C_2 \sum A \frac{y}{D} \sin^2 \alpha \quad (3)$$

Where C_1 is an empirical coefficient (C_1 = 1.40 for normal weight concrete); C_2 empirical coefficient (C_2 = 300 N//mm^2 for deformed bars, 130 N//mm^2 for plain round bars, and 105 N//mm^2 for GFRP bars); D is the overall depth of deep beam; f_t is cylinder splitting tensile strength of concrete $\left(0.6\sqrt{f_{cu}}\ \text{N/mm}^2\right)$; y depth at which a typical bar intersects the potential critical diagonal crack; α angle of intersection between a typical bar and potential critical diagonal crack; b is the breadth of the deep beam; f_{cu} Cube strength of concrete; A area of an individual web bar and longitudinal bars. The authors used in this paper C_2 = 105 N//mm^2 for GFRP bars, and this value was predicted by iteration in equation 3. Table 7 shows the prediction result for ultimate shear capacity using Eq. (3).

The authors modified the equation produced by Kong *et al.* to get the best estimation for tested specimens, and

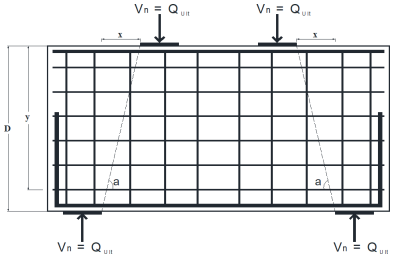

Figure 21: Natural load paths joining the loading and reaction points

Table 7: Measured and computed ultimate load deep beams

Specimens ID	C_1 [1-0.35(x/D)] f_t b D (kN)	$C_2 \Sigma$ A (y/D) $\sin^2 \alpha$ (kN)	V_n (kN)	$V_{u\,equ.}$ (kN)	$V_{u\,exp.}$ (kN)	$V_{u\,exp.}/V_{u\,equ.}$ %
BS1	377	106	482	964	554	0.57
BS2	377	126	503	1006	665	0.66
BS3	377	140	517	1034	690	0.67
BG1	377	91	467	935	571	0.61
BG2	377	127	503	1007	585	0.58
BG3	377	113	490	980	630	0.64
BG4	377	102	479	957	580	0.61

Note: C_2 = 130 N//mm^2 for steel bars, C_2 = 105 N//mm^2 for GFRP bars

Table 8: Measured and computed ultimate load deep beams by using modified equation by authors

Specimens ID	$\frac{1}{10}\left[1-0.35\,\frac{x}{D}\right] f'_c bD$ (kN)	$C_2 \Sigma$ A (y/D) $\sin^2 \alpha$ (kN)	V_n (kN)	$V_{u\,equ.}$ (kN)	$V_{u\,exp.}$ (kN)	$V_{u\,exp.}/V_{u\,equ.}$ %
BS1	179	106	285	570	554	0.97
BS2	179	126	306	611	665	1.09
BS3	179	140	319	639	690	1.08
BG1	179	91	270	540	571	1.06
BG2	179	127	306	612	585	0.96
BG3	179	113	292	585	630	1.08
BG4	179	102	281	563	580	1.03

Note: C_2 = 130 N//mm^2 for steel bars, C_2 = 105 N//mm^2 for GFRP bars

Table 8 shows the predicted result for ultimate shear capacity. Furthermore, the modified equation is as follows:

$$V_n = \frac{1}{10}\left[1 - 0.35\frac{x}{D}\right] f'_c bD + C_2 \sum A \frac{y}{D} \sin^2 \alpha \quad (4)$$

6.2 Strut-tie model

The strut-tie model is used to design concrete structural regions or members where geometric discontinuities or loads cause a nonlinear distribution of strain or stress within the member cross-section, and the members or regions represent an idealized truss. D-region design and analysis using a hypothetical pin-jointed truss consisting of ties and struts connected at nodes in strut-tie-model theory. The secondary effect, such as moment, is not included in the strut-tie-model. In an idealized truss, a strut serves as a compression member, the tie assigned as tension member, and the nodes as joints. Similarly, a set of discrete ties represents a collection of individual bars or wires. Concrete surrounds the ties, reducing elongation and defining the force anchoring zone [19–23]. Figure 22 shows the width of the strut and tie. The angle between strut and tie axes should not be less than 25°, as recommended by ACI 318-19 in chapter 23.2.7.

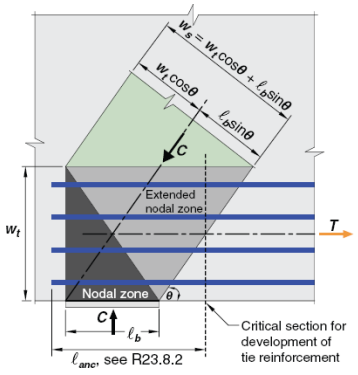

Figure 22: Reinforcement distribution

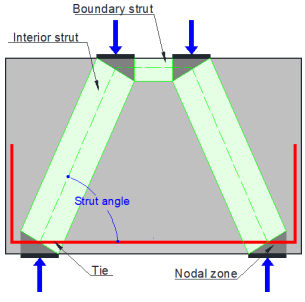

Figure 23: Description of strut-tie-model

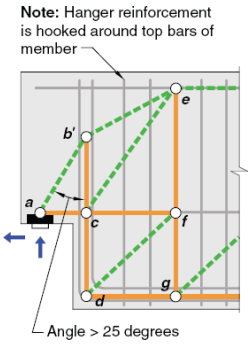

Figure 24: Adjusted strut-tie-model to satisfy 23.2.7

6.2.1 ACI 318-19 recommendation for using strut-tie-model

The nominal compressive strength of the strut F_{ns} in ACI 318-19 is presented in the following formula:

$$F_{ns} = f_{ce}A_{cs} \tag{5}$$

Where: F_{ns} is calculated at the end of the strut and taken as lesser value; A_{cs}; is the cross-sectional area of the strut; f_{ce}; is the effective compressive strength of the concrete.

$$f_{ce} = 0.85\beta_c\beta_s f'_c \tag{6}$$

Where: β_s, β_c; is per ACI 318-19 Table 23.4.3(a) and Table 23.4.3(b), respectively. The coefficient 0.85 f'_c; represent the effective concrete strength under compression force.

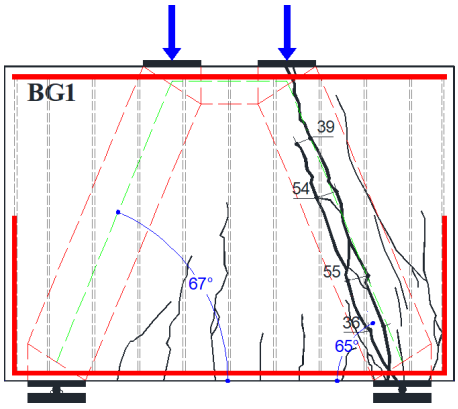

Figure 26: Crack pattern and mode of failure for horizontal web reinforcement only with ratio 0.40%

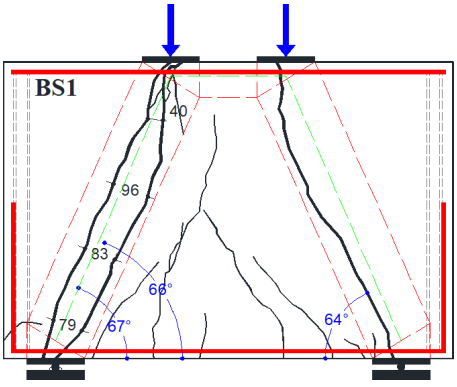

Figure 25: Crack pattern and mode of failure for a deep beam without web reinforcement

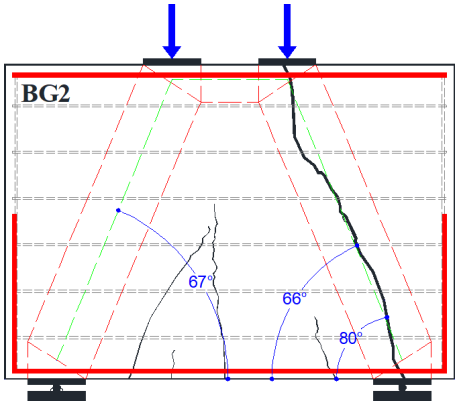

Figure 27: Crack pattern and mode of failure for vertical web reinforcement only with ratio 0.40%

Table 9: Design of deep beams with strut and tie method

Specimen ID	$V_{uexp.}$ (kN)	Θ	F_{ns} (kN)	F_{nt} (kN)	β_n	W_t (mm)	L_{anc} (mm)	F_{nn} (kN)	W_s (mm)	W_{st} (mm)
BS1	554	66	303.2	123.3	0.8	83	164	252	171	149
BS2	665	71	351.7	114.5	0.8	77	159	244	167	145
BS3	690	68	372.1	139.4	0.8	94	162	248	174	160
BG1	571	65	315.0	133.1	0.8	90	166	254	174	155
BG2	585	80	297.0	51.6	0.8	35	152	234	154	107
BG3	630	66	344.8	140.2	0.8	95	164	252	175	160
BG4	580	68	312.8	117.2	0.8	79	162	248	169	146

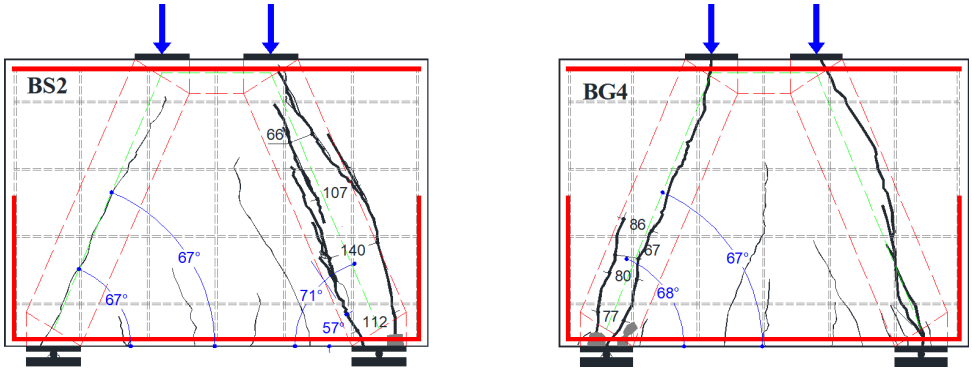

Figure 28: Crack pattern and mode of failure for web reinforcement ratio 0.25% (shaded area indicates crushed concrete)

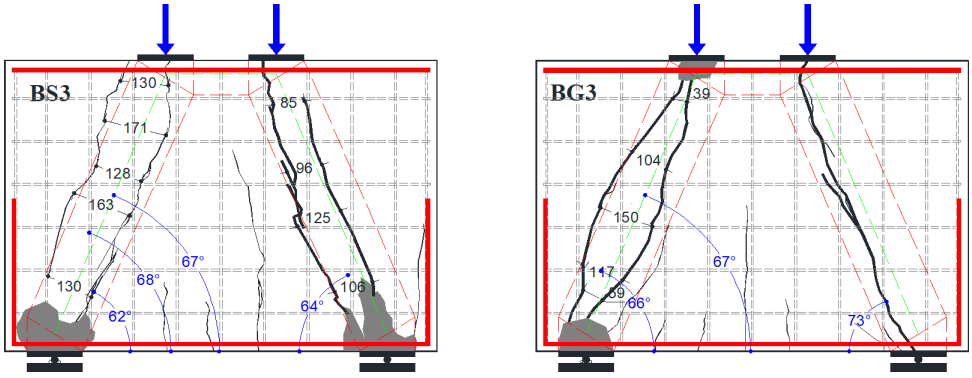

Figure 29: Crack pattern and mode of failure for web reinforcement ratio 0.40% (shaded area indicates crushed concrete)

The nominal tension strength of the tie F_{nt} is presented in the following formula:

$$F_{nt} = f_y A_{ts} \tag{7}$$

The effective width w_t of the tie can be calculated as $w_t = d_{bar} + 2C_p$ (bar diameter + twice concrete cover). If the reinforced bars are distributed uniformly in a single layer, the width of the tie is the width corresponding to the width in a hydrostatic nodal zone. The maximum width of the tie $w_{t,max}$ can be taken from the following formula; where f_{ce}; is taken from the formula calculated for the nodal zone (per ACI 318-19 section 23.9.2).

$$w_{t,max} = \frac{F_{nt}}{f_{ce} b_s} \tag{8}$$

F_{nn} is the nominal compressive strength of nodal zone and shall be calculated by:

$$F_{nn} = f_{ce} A_{nz} \tag{9}$$

$$f_{ce} = 0.85 \beta_c \beta_n f_c' \tag{10}$$

Where: β_n, β_c Per ACI 318-19 Table 23.9.2 and Table 23.4.3(b), respectively.

The strut and tie model theory assumes that a portion of a reinforced concrete structure uses hypothetical pin-jointed trusses consisting of struts and ties connected at nodes. The deep beam without web reinforcement the compression concrete strut formed between load point and support with inclination angle $\theta = 66^\circ$ and formed as prismatic strut with average width 90 mm at mid-length of the strut, another strut not formed until failure of the deep beam, an only shear crack formed with inclination angle $\theta = 64^\circ$, the strut width at top decreased to half-width at mid of strut as shown in Figure 25, the width of the strut was less than the design with ACI-318-19 as shown in Table 9.

As shown in Figures 26 and 27, the deep beam that reinforced with GFRP as web reinforcement as a vertical-only with the ratio of 0.40%, only one strut formed as a prismatic during the test with inclination angle $\theta = 65^\circ$ And average width at mid of strut 55 mm. The beam with only horizontal web reinforcement with a ratio of 0.40%, no concrete strut was formed until failure of the beam, only shear crack with formed with inclination angle $\theta = 80^\circ$.

The reinforced concrete deep beam with steel web reinforcement ratio 0.25%, only on strut formed as a bottled shape with inclination angle $\theta = 71^\circ$, in another side of the deep beam, a shear crack was formed with angle $\theta = 67^\circ$.

Furthermore, minor crashing in the bottom nodal zone, the width of the strut was 140 mm at mid of strut, 66, 112 mm at top and bottom of the strut; respectively. The deep beam with GFRP web reinforcement ratio 0.25%, a crashing has occurred in the bottom nodal zone, only one strut as prismatic strut with inclination angle $\theta = 68^{\circ}$. The strut's average width was approximately 85 mm, and on another side of the deep beam, a shear crack formed until it failed during the test. The GFRP did not affect the crack angle of the deep beam, as illustrated in Figure 28.

Figure 29 shows the deep beam reinforced with a steel web reinforcement ratio of 0.40%, no crushing occurred beneath the loading in the top nodal zone, but a crushing occurred in both struts at the bottom nodal zone; the two struts as prismatic strut formed during the test with different widths at the middle, top, and bottom of both struts. The deep beam was reinforced with GFRP as web reinforcement with a ratio of 0.40%, only one strut formed, the other side of the deep beam was a shear crack, and crushing occurred in the bottom nodal zone of the strut.

6.2.2 Strut-tie model according to ACI 318-19 (CAST software)

CAST software developed a strut-tie model for a tested deep beam. Many iterations were performed on CAST to get a suitable strut tie model and a high ultimate load. All struts'

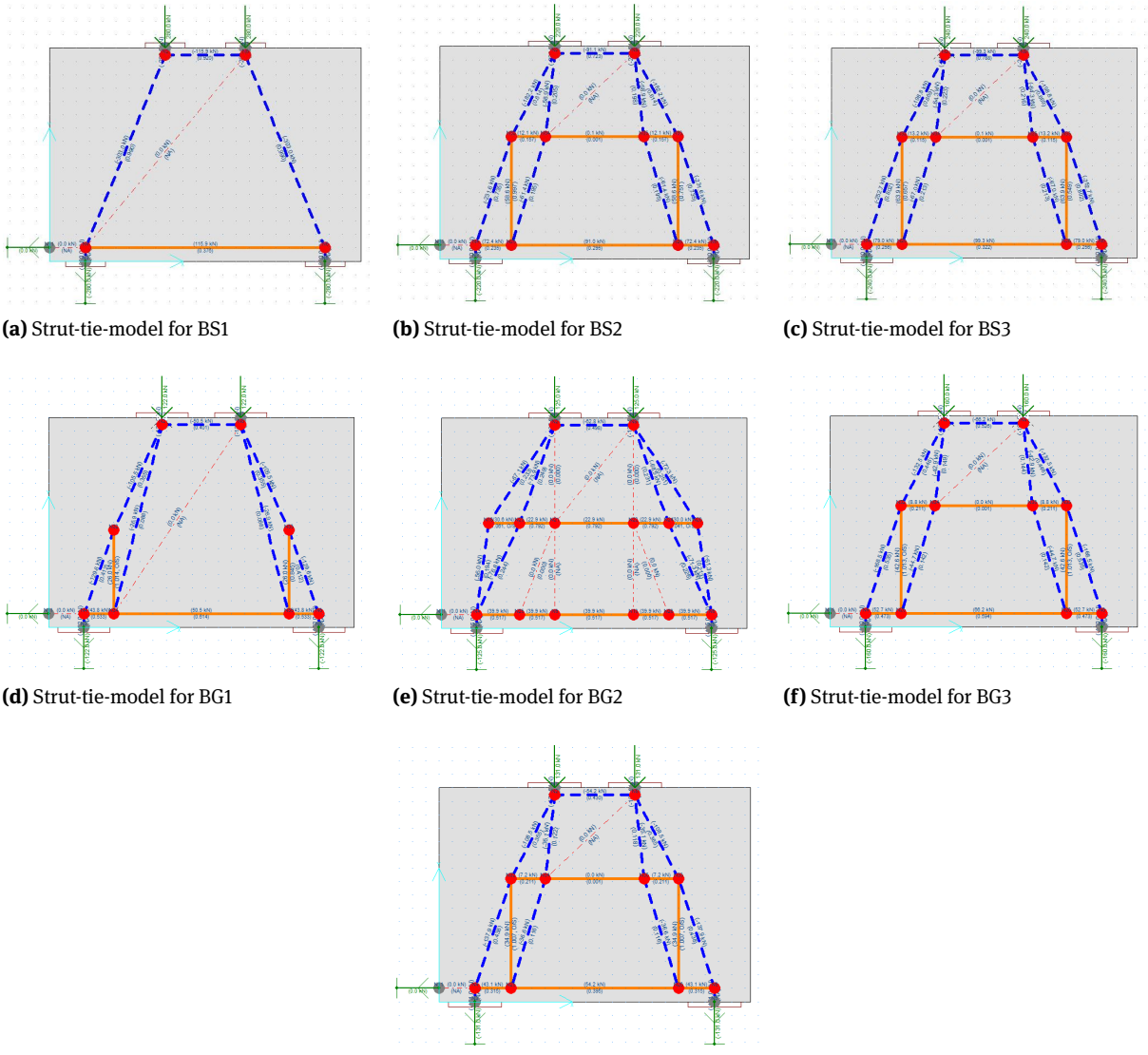

(a) Strut-tie-model for BS1

(b) Strut-tie-model for BS2

(c) Strut-tie-model for BS3

(d) Strut-tie-model for BG1

(e) Strut-tie-model for BG2

(f) Strut-tie-model for BG3

(g) Strut-tie-model for BG4

Figure 30: Stress ratios in strut-tie-model accordance to ACI 318-19

Table 10: Cast ultimate capacity according to ACI 318-19

Specimen ID	Maximum stress ratio					Failure location	$V_{n\ pre.}$ kN	$V_{n\ exp.}$ kN	$\frac{V_{n\ exp.}}{V_{n\ pre.}}$
	Tie	Strut	Node	Horizontal web	Vertical web				
BS1	0.36	1.00	0.93	—	—	Concrete Strut	560	554	0.98
BS2	0.29	0.75	0.92	0.16	1.00	Vertical Tie	445	665	1.49
BS3	0.32	0.80	1.00	0.15	0.66	Node-CTT	480	690	1.43
BG1	0.15	0.41	0.39	—	1.00	Vertical Tie	245	571	2.33
BG2	0.13	0.25	0.37	1.00	—	Horizontal Tie	250	585	2.34
BG3	0.22	0.54	0.67	0.21	1.00	Vertical Tie	320	630	1.96
BG4	0.18	0.44	0.55	0.21	1.00	Vertical Tie	262	580	2.21

$V_{exp.}$ = experimental ultimate shear strength, $V_{pre.}$ = predicted ultimate shear capacity.

Table 11: Design of deep beams with traditional ACI design method (ACI 318R-99) [17]

Specimen ID	Web Reinf. Type	ρ_h%	ρ_v%	V_s	V_c	$V_{n\ \max}$	V_u	$V_{n\ pre.}$	$V_{n\ exp.}$	$\frac{V_{n\ exp.}}{V_{n\ pre.}}$
BS1	Steel	0	0	0	67.7	262.46	262.46	524.9	554	1.06
BS2		0.25	0.25	80.028	67.7	262.46	342.488	685.0	665	0.97
BS3		0.40	0.40	128.04	67.7	262.46	390.5	781.0	690	0.88
BG1	GFRP	0	0.40	5.67	67.7	262.46	268.13	536.3	571	1.06
BG2		0.40	0	26.66	67.7	262.46	289.12	578.2	585	1.01
BG3		0.40	0.40	31.95	67.7	262.46	294.41	588.8	630	1.07
BG4		0.25	0.25	20.06	67.7	262.46	282.52	565.0	580	1.03

$V_{exp.}$ = experimental ultimate shear strength (kN), $V_{pre.}$ = predicted ultimate shear capacity (kN), Reinf.= reinforcement

angles are more than 25°, some members in the strut-tie-model used as stabilizer members. GFRP web reinforcement design calculations have been performed per ACI 440.1R-03 using the equations shown below. Figure 30 shows the stress ratio in strut-tie-model members, and Table 10 shows the ultimate shear capacity result.

$$f_{fb} = \left(0.05\frac{r_b}{d_b} + 0.3\right) f_{fu} \le f_{fu} \tag{11}$$

$$f_{fv} = 0.002E_f \le f_{fb} \tag{12}$$

Where f_{fb}; is the design tensile strength of the bend of GFRP bar, Mpa; r_b is the radius of the bend, mm.; d_b the diameter of reinforcing bar, mm.; and f_{fu} the design tensile strength of GFRP, considering reductions for service environment, Mpa; f_{fv} the design stress for GFRP web reinforcement and it used equal 90 Mpa; E_f; is the guaranteed modulus of elasticity of GFRP.

6.3 ACI traditional design method (ACI 318R-99)

The deep beam's sectional shear strength was determined using Section 11.8 of the ACI 318R-99 [17] Code by summing the contributions of the concrete and the distributed vertical and horizontal reinforcement. Both the concrete and steel contributions have various expressions and limits. Eq. (13) and Eq. (14) calculate the maximum shear and shear strength, respectively. In this paper, Eq. (13) was used to calculate the maximum capacity of the deep beam to compare it with tested specimens at the maximum point of loading. When the factored shear force V_u at the critical section exceeds the shear strength $\varnothing V_c$, shear reinforcement is required (Section 11.8.8, ACI 318R-99), Eq. (15) calculate the contribution of shear reinforcement. Eq. (16) calculates the ultimate shear capacity for the deep beam, and Table 11 shows the results of ultimate shear capacity. The design stress f_{fv} for GFRP web reinforcement was calculated using Eq. (11) and Eq. (12).

$$V_{n\ \max} = \varnothing 0.66\sqrt{f'_c}\, b_w d \tag{13}$$

$$\varnothing V_c = \varnothing 0.17\sqrt{f'_c}\, b_w d \tag{14}$$

$$V_s = \left[\frac{A_v}{S_v}\left(\frac{1 + l_n/d}{12}\right) + \frac{A_h}{S_h}\left(\frac{11 - l_n/d}{12}\right)\right] f_y d \quad (15)$$

$$V_u = V_{n\ \max} + V_s \quad (16)$$

Where: $V_{n\ \max}$; maximum nominal concrete shear strength (Mpa), f'_c; specified concrete compressive strength (Mpa), b_w; cross-section width of deep beam (mm), d; cross-section depth of deep beam (mm), $\varnothing V_c$; factored nominal concrete shear strength (Mpa), V_s; nominal shear strength provided by shear reinforcement Mpa, A_v; area of vertical shear reinforcement (mm^2) with a distance S_v (mm), A_h; area of horizontal shear reinforcement (mm^2) with a distance S_h (mm), l_n; clear span between supports (mm), V_u; ultimate shear capacity (Mpa). $\varnothing$; reduction factor.

6.4 Numerical model

The nonlinear finite element technique (F.E) was utilized in this work to predict the behavior of simply supported reinforced concrete deep structures using the ABAQUS 6.13.1 software, the deep beam was reinforcement with glass fiber reinforced polymer (GFRP) as web reinforcement with different ratios, and the main reinforcement were steel bars. The load was applied as a concentrated load in the middle of the steel plate as P/2. One support prevents the movement in X, Z direction and prevents the translation in the Y direction to act as pin support; the second support prevents the movement in the X direction and prevents translation in the Y direction to act as roller support.

6.4.1 Concrete damaged plasticity (CDP) model and utilized material properties

In this study concrete damaged plasticity (CDP) model will be used to represent concrete behavior in finite element analysis using the ABAQUS program. CDP model was used in compression and tension to replicate concrete's inelastic behavior with damaged characteristics. The total strain tensor comprised of the elastic part ϵ and the plastic part ϵ^{el}. The concrete behavior explained by ϵ^{pl}assuming that the concrete damage plasticity utilized the yield function $f\left(\epsilon^{pl,h},\ \bar{\sigma}\right)$; which represented the yield surface in effective stress space to determine the states of damage or failure.

$$\sigma_c = (1 - d_c)\, E_0 \left(\epsilon_c - \epsilon_c^{pl,h}\right) \quad (17)$$

The tensile response of concrete concerning the concrete plasticity model subjected to tension load was given by:

$$\sigma_t = (1 - d_t)\, E_0 \left(\epsilon_t - \epsilon_t^{pl,h}\right) \quad (18)$$

Where: d_c and d_t, two scalar damage variables, ranging from 0 (undamaged) to 1 (fully damaged), E_0, ϵ_c, ϵ_t, $\epsilon_c^{pl,h}$, $\epsilon_t^{pl,h}$. The initial elasticity modulus, the concrete compressive strain, the concrete tensile strain, the concrete plastic compressive strain, and the concrete plastic tensile strain, respectively.

$$\epsilon_c^{pl,h} = \epsilon_c^{in,h} - \frac{\sigma_c}{E_0}\left(\frac{d_c}{1 - d_c}\right) \quad (19)$$

$$d_c = 1 - \frac{\sigma_c}{\sigma_{cu}} \quad (20)$$

In uniaxial concrete tensile behavior, the plastic hardening in tension $\epsilon_t^{pl,h}$ was derived as follows:

Table 12: Concrete parameters in ABAQUS

E_c	υ	ψ	ϵ	σ_{b0}/σ_{c0}	K_c
22500	0.2	40	0.10	1.16	0.667

$$\epsilon_t^{pl,h} = \epsilon_t^{ck,h} - \frac{\sigma_t}{E_0}\left(\frac{d_t}{1 - d_t}\right) \quad (21)$$

$$d_t = 1 - \frac{\sigma_t}{\sigma_{to}} \quad (22)$$

Where: E_c, υ, ψ, ϵ, σ_{b0}/σ_{c0}, K_c Concrete elastic modulus (MPa), Poisson's ratio, Dilation angle, Flow potential eccentricity, the ratio of initial equibiaxial compressive yield stress to initial uniaxial compressive yield stress, and the coefficient determining the shape of the deviatoric concrete cross-section; respectively. Figure 37 illustrates the crack pattern. Figure 33 shows the load-deflection curve produced by the Finite element method (AAQUS 6.13), and Figures 34 to 36 illustrate the strain for bars.

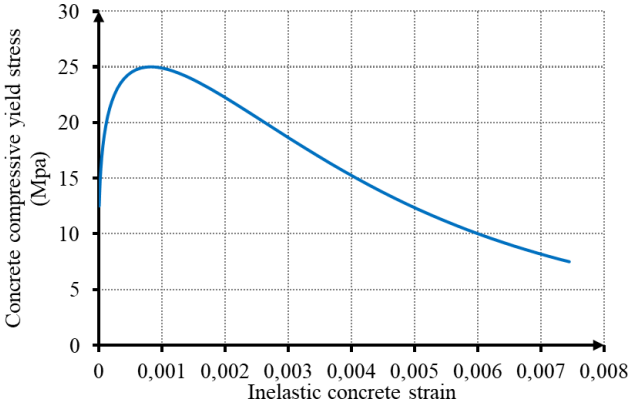

Figure 31: The relation between concrete compressive stress and inelastic concrete strain used in ABAQUS for tested specimens

Table 13: Summary of experimental and numerical results loads (ABAQUS 6.13)

Specimen ID	Ultimate load (kN)		First flexural crack (kN)		First Shear crack (kN)		Main diagonal crack (kN)		$\frac{V_{n\ exp.}}{V_{n\ pre.}}$
	$P_{u\ E.}$	$P_{u\ N.}$	$P_{f\ E.}$	$P_{f\ N.}$	$P_{s\ E.}$	$P_{s\ N.}$	$P_{cr\ E.}$	$P_{cr\ N.}$	
BS1	554	534	360	335	480	516	530	534	1.04
BS2	665	633	396	391	396	466	665	630	1.05
BS3	690	712	310	438	450	485	670	680	0.97
BG1	571	544	352	350	352	470	571	495	1.05
BG2	585	549	330	386	375	500	585	520	1.07
BG3	630	600	360	360	400	485	465	530	1.05
BG4	580	570	312	365	346	500	537	510	1.02

Note: Letter E for experimental specimens and letter N for numerical modeling

Table 14: Summary of experimental and numerical results

Specimen ID	Flexural crack depth (mm)		Strut shape	
	$D_{f\ E.}$	$D_{f\ N.}$	Experimental	Numerical
BS1	650	140	Prismatic	Diagonal crack
BS2	520	175	Bottled	Prismatic
BS3	520	245	Prismatic	Prismatic
BG1	400	175	Prismatic	Prismatic
BG2	420	140	Diagonal crack	Prismatic
BG3	380	245	Bottled	Prismatic
BG4	500	175	Prismatic	Prismatic

Table 15: Prediction of ultimate shear strength

Beam ID	$V_{exp.}$	Kong et al.		Kong et al. (Modified by authors)		ACI 319-19 (CAST Software)		ACI traditional method (ACI 318R-99)		Finite element method (ABAQUS 6.13)	
		$V_{pre.}$	$V_{exp.}/V_{pre.}$	$V_{pre.}$	$V_{exp.}/V_{pre.}$	$V_{pre.}$	$V_{exp.}/V_{pre.}$	$V_{pre.}$	$V_{exp.}/V_{pre.}$	$V_{pre.}$	$V_{exp.}/V_{pre.}$
BS1	554	964	0.57	570	0.97	560	0.98	524.9	1.06	534	1.04
BS2	665	1006	0.66	611	1.09	445	1.49	685.0	0.97	633	1.05
BS3	690	1034	0.67	639	1.08	480	1.43	781.0	0.88	712	0.97
BG1	571	935	0.61	540	1.06	245	2.33	536.3	1.06	544	1.05
BG2	585	1007	0.58	612	0.96	250	2.34	578.2	1.01	549	1.07
BG3	630	980	0.64	585	1.08	320	1.96	588.8	1.07	600	1.05
BG4	580	957	0.61	563	1.03	262	2.21	565.0	1.03	570	1.02

$V_{exp.}$ = experimental ultimate shear strength (kN), $V_{pre.}$ = predicted ultimate shear strength (kN)

7 Comparison of experimental and predicted results

Table 15 shows the calculated ultimate shear strengths for the tested beams with various web reinforcement ratios based on the above models and equations. In Figure 38, the experimental and predicted ultimate shear strengths $\frac{V_{exp.}}{V_{pre.}}$ ratios plotted for the beams. There are overestimations in the predictions produced by Kong et al. has shown the ultimate strength for the deep beams. The ultimate strength of deep beams predicted using the ACI 318-19 gives a high conservative prediction, and the ACI 318-19 appears to be more conservative for deep beams reinforced with GFRP shear reinforcement. As a result, required new expressions to temper the excessive conservatism. The modified equation by

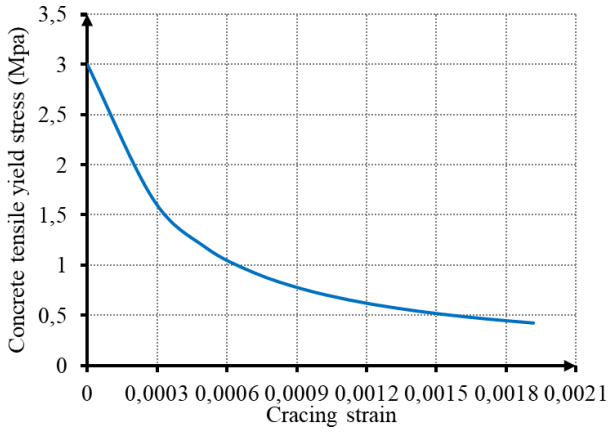

Figure 32: The relation between concrete tensile stress and concrete cracking strain used in ABAQUS for tested specimens

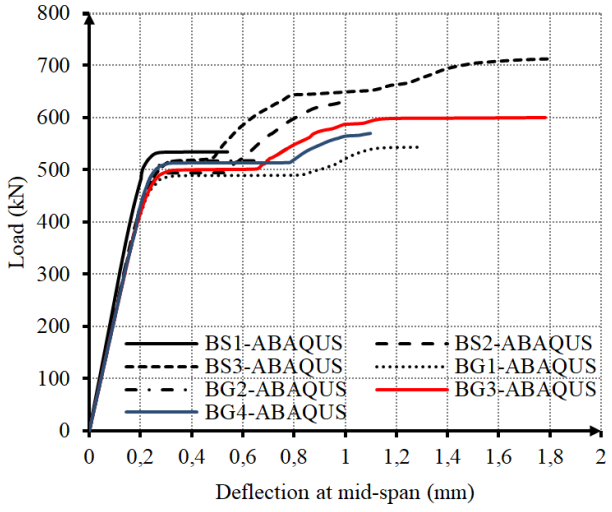

Figure 33: Load-deflection curve for deep beams

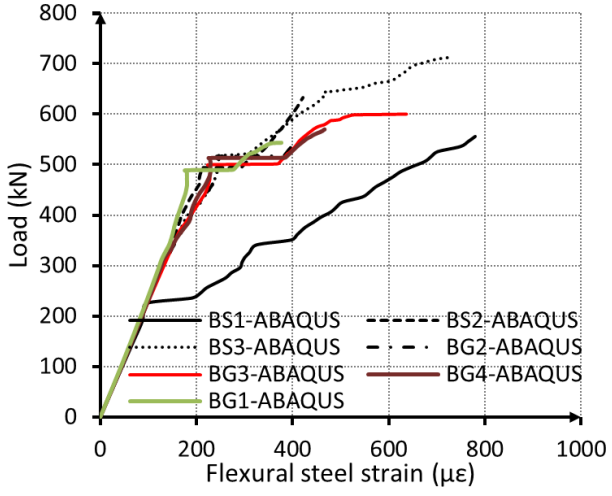

Figure 34: Strain curve for deep beams' main bar (Tie)

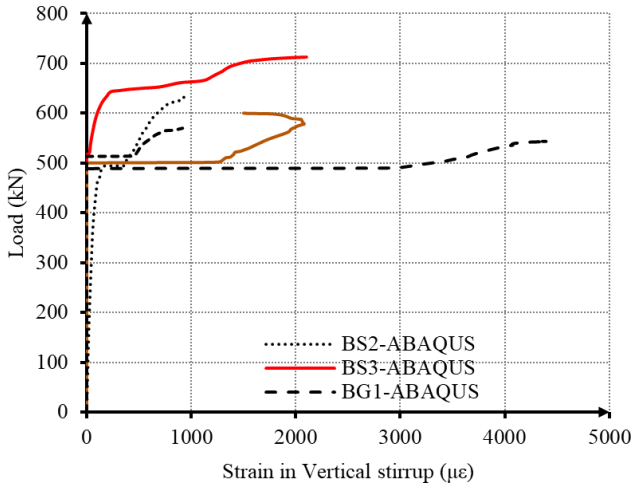

Figure 35: Strain curve of vertical web reinforcement for deep beams

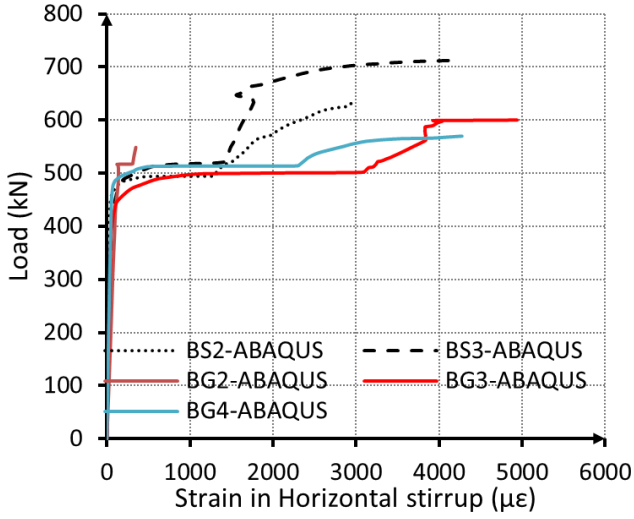

Figure 36: Strain curve of horizontal web reinforcement for deep beams

authors that produced by Kong *et al.*, ACI traditional design method (ACI 318-99) and finite element method (ABAQUS 6.13) based shear strength prediction produced the best estimation of ultimate shear capacity for deep beams with various web reinforcement ratios; the mean value of $\frac{V_{exp.}}{V_{pre.}}$ was 1.04 for modified equation produced by Kong *et al.*, 1.01 for ACI ACI traditional design method (ACI 318-99), and 1.03 for Finite element method (ABAQUS 6.13).

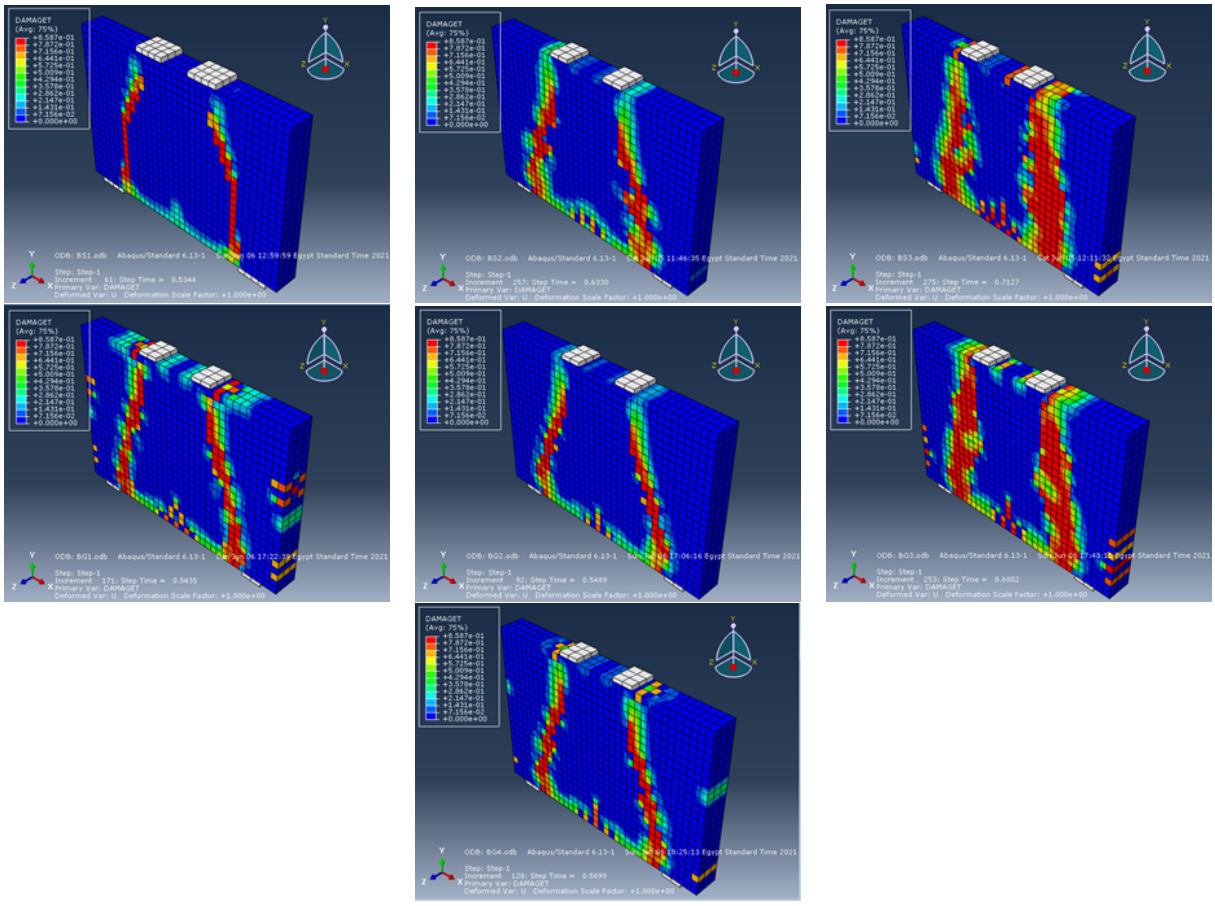

Figure 37: Crack development and mode of failure

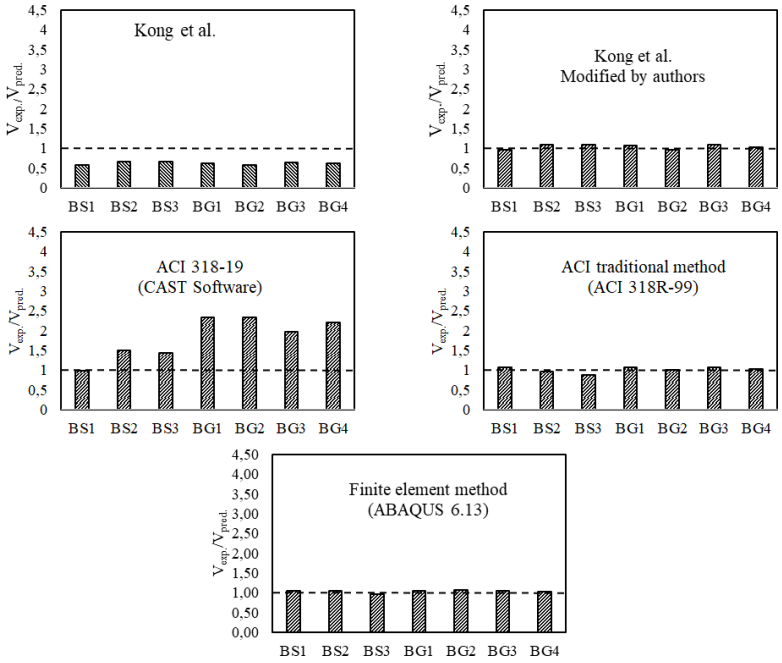

Figure 38: Ratios between Experimental to predicted ultimate shear strength of tested specimens

8 Conclusion

The purpose of this study was to examine the behavior of deep beams reinforced with hybrid glass fiber reinforced polymer (GFRP) as web reinforcement and with steel bars as primary deep beam reinforcement, with an emphasis on the effect of web reinforcement on such structural elements. The experimental program consisted of seven specimens=, and seven deep beams were studied using the numerical software ABAQUS. All deep beams had a span to depth ratio (a/d) of 0.40, and various web reinforcement configurations were tested and investigated to accomplish this goal. The following conclusion can be reached based on the test results and analysis:

- All experimental specimens exhibited almost bilinear deflection response up to failure.
- The deep beams with a web reinforcement ratio of 0.40% had almost similar stiffness up to the initial crack.
- The failure mode for all experimental and numerical modeling was a shear failure.
- No effect on cracking load, flexure load, and shear load; the reinforcement ratio affects only the ultimate load capacity of the deep beams.
- The type of web reinforcement did not affect the number of bending cracks but affected shear cracks.
- The energy absorption decreased for the tested deep beam when the web reinforcement increased.
- The ductility index and deformability factor decreased by web reinforcement increased.
- The deep beam stiffness at initial and maximum load increased by web reinforcement but decreased at failure.
- The Finite element method predicted The experimental response of the tested beams. However, more work in the used Finite element software is required to predict the failure point load directly.
- When the experimental shear strengths were compared to the predicted values using the available equations and models in the literature, the modified equation for Kong *et al.*, ACI traditional design method (ACI 318R-99), and Finite element method (ABAQUS 6.13)-based shear strength methods produced the most accurate results. Other models and equations produced either unsafe estimation (Kong *et al.*) or excessive underestimation of the ultimate strength for deep beams with various web reinforcement ratios (The ACI 318-19).

Funding information: The authors state no funding involved.

Author contributions: All authors have accepted responsibility for the entire content of this manuscript and approved its submission.

Conflict of interest: The authors state no conflict of interest.

References

[1] Farghaly AS, Benmokrane B. Shear behavior of FRP-reinforced concrete deep beams without web reinforcement. J Compos Constr. 2013;17(6):10.
[2] Ţăranu N, Oprişan G, Isopescu D, Enţuc I, Munteanu V, Banu C. Fiber reinforced polymer composites as internal and external reinforcements for building elements. Bulletin of the Polytechnic Institute of Jassy – Construction, Architecture Section. 2008:7-20.
[3] Mohamed KA. Performance and strut efficiency factor of concrete deep beams reinforced with GFRP bars [dissertation]. Quebec: University of Sherbrooke; 2015:184.
[4] ElSafty A, Benmokrane B, Rizkalla S, Mohamed H, Hassan M. Degradation assessment of internal continuous fiber reinforcement in concrete environment. Technical Report. Tallahassee (FL), USA; 2014. p. 297.
[5] Rogowsky DM, MacGregor JG. Shear strength of deep reinforced concrete continuous beams. Structural Engineering Report No. 110. Edmonton: University of Alberta; 1983 p. 178.
[6] Mohamed K, Farghaly AS, Benmokrane B. Effect of vertical and horizontal web reinforcement on the strength and deformation of concrete deep beams reinforced with GFRP bars. ASCE J Struct Eng. 2017;143(8).
[7] Andermatt MF, Lubell AS. Behaviour of concrete beams with internal GFRP reinforcement. In: Bartlett FM, editor. Proceedings of 8th International Conference on Short and Medium Span Bridges; 2010 Aug 3-6; Niagara Falls, Canada. Canadian Society for Civil Engineering; 2010. p. 260–261.
[8] American Concrete Institute (ACI). Report on fiber-reinforced polymer (FRP) reinforcement concrete structures (ACI 440R-07). ACI, Farmington Hills, MI. 2007.
[9] Fédération Internationale du Béton (FIB). FRP reinforcement in RC structures. Task Group 9.3, Lausanne, Switzerland. 2007.
[10] Mohamed HM, Benmokrane B. Design and performance of reinforced concrete water chlorination tank totally reinforced with GFRP bars: Case study. J Compos Constr. 2014;18(1).
[11] Tan KH, Kong FK, Teng S, Weng LW. Effect of web reinforcement on high-strength concrete deep beams. ACI Struct J. 1997a;94(5):572–82.
[12] Mihaylov BI, Bentz EC, Collins MP. Behavior of large deep beams subjected to monotonic and reversed cyclic shear. ACI Struct J. 2010;107(6):726–34.
[13] Birrcher DB, Tuchscherer RG, Huizinga M, Bayrak O. Minimum web reinforcement in deep beams. ACI Struct J. 2013;110(2):297–306.

[14] American Concrete Institute (ACI). Building code requirements for structural concrete (ACI 318-14). ACI, Farmington Hills, MI. 2014.
[15] American Concrete Institute (ACI). Building code requirements for structural concrete (ACI 318-19 and ACI 318R-19). ACI, Farmington Hills, MI. 2019:628.
[16] American Concrete Institute (ACI). Guide for the design and construction of concrete reinforced with FRP bars (ACI 440.1R-03). ACI, Farmington Hills, MI. 2003:42.
[17] American Concrete Institute (ACI). Specifications for structural concrete (ACI 301-99). ACI, Farmington Hills, MI.1999:49.
[18] Kong FK, Sharp GR, Appleton SC, Beaumont CJ, Kubik LA. Structural idealization for deep beams with web openings: Further evidence. Magazine Concr Res. 1978;30(103):89–95.
[19] Ghoneim M, El Mihilmy M. Design of reinforced concrete structures. 1st ed. Oxford University Press. 2008. p. 817.
[20] Schlaich J, Schäfer K. Design and detailing of structural concrete using strut-and-tie models. Struct Eng. 1991;69(6):113–25.
[21] Mitchell D, Collins MP, Bhide SB, Rabbat BG. AASHTO LRFD Strut-and-Tie Model Design Examples. 1st ed. Skokie (IL): Portland Cement Association; 2004. p. 60.
[22] Brown MD, Bayrak O. Minimum Transverse Reinforcement for Bottle-Shaped Struts. ACI Struct J. 2006;103(6):813–21.
[23] ACI Committee 440. Guide for the Design and Construction of Concrete Reinforced with FRP Bars (ACI 440.1R-06). ACI, Farmington Hills, MI. 2006: 44.